# Optimized Performance of Cap and Pin Insulator under Wet Pollution Conditions Using a Mono-Objective Genetic Algorithms

## D. Doufene, S. Bouazabia
Electrical and Industrial Systems Laboratory (LSEI)
University of Science and Technology Houari Boumediene (USTHB)
BP 32 El Alia 16111,
Bab Ezzouar 16111, Algiers, Algeria
## A. Haddad
Advanced High Voltage Engineering Research Centre
School of Engineering, Cardiff University
Cardiff CF24 3AA, UK

## ABSTRACT
**Extensive research was carried out on the relation between pollution performances of high voltage ceramic insulators and their shape. However, very little work is published using numerical optimization methods.**
**In this paper, we propose an alternative approach for optimizing ceramic insulators shapes by adopting an optimization numerical approach, namely the genetic algorithms technique combined with the finite element method for electrical field and leakage current density calculation. The objective is to compare the pollution performance of an industrial (reference) cap and pin insulator with its optimized model obtained usinga genetic algorithms optimization method. The impact of the insulator shape and the pollution on the electrical parameters (voltage, electric field and conduction current density distributions) are quantified. In this work, it was shown that the optimized shape performs better than the exiting equivalent units when the pollution is deposited near to high voltage terminal located at the pin of a cap-and-pin insulator.**

Index Terms —**Insulation, Pollution, Electric field, Finite element method (FEM), Optimization, Genetic algorithms.**

## 1 INTRODUCTION

**THE** reliability of electrical power systems is strongly dependent on the continuous satisfactory performance of all its constituent equipment, and one of the most crucial elements amongst these is the outdoor insulator used in overhead transmission and distribution lines. Cap and pin insulators have been in use since the early days of power networks. During their service life, these insulators are able to withstand not only the operating voltage but also over voltages and flashover events, in addition to the mechanical stresses [1, 2].

Due to their outdoor installation, insulators are always subjected to the elements; in particular, various types and levels of surface pollution, such as industrial, saline, dust and agricultural particulates [3]. It is now well established that the performance of outdoor insulators is strongly affected by this environmental contamination [4]. When this pollution layer is wetted under humid conditions, insulator flashover becomes the main problem which threatens continuity of power supply [5] and the flashover mechanism is now fairly well understood [6]. It is established that the wetting of the pollution layer with high humidity, fog or light rain, lowers its resistance and becomes

conducting, giving rise to leakage current flow in the pollution layer on the insulator surface [7]. This current flow is not uniform due to the shape of the insulator and the non-uniform repartition of the pollution layer on the insulator surface. As a consequence, regions of high current density exist on the insulator surface and are associated with higher local power dissipation, e.g. close to the pin in the case of a cap and pin insulator. This localised heating contributes to the formation of dry bands on the surface [8] and leads to arc formation across it. Such partial arcing can grow in length or join with others to develop a full flashover.

Several techniques were developed and applied to mitigate insulator pollution flashover; e.g. periodic washing [9,10], greasing and coating with water-repellent agents and materials [11,12], increasing the creepage length of the insulator strings [13,14], and improvement of insulator design [15]. This pollution flashover performance of insulators is one of the guiding factors in their design and dimensioning for outdoor application on power lines [3,16]. Furthermore, earlier research, focussed on improving the insulator design under polluted conditions, led to the widely adopted anti fog profile for

polymeric insulators [17] and the adoption of permittivity graded materials [18]. However, there is very little published material using numerical optimization methods to improve the design [19–24], but with no investigation of polluted insulator case.

IEC 608015 [25] gives three approaches of dimensioning insulators; (a) using past experience, (b) measure and test and (c) measure and design.

In this paper, a new approach for dimensioning ceramic insulators by mean of a numerical method of optimization, namely, the Genetic Algorithms (GA) method combined with Finite Element method, is proposed.

The Genetic Algorithms method is widely adopted in various areas. It is based on the evolutionary ideas of natural selection and genetics, and it is an adaptive heuristic search technique for solving both constrained and unconstrained optimization problems [26, 27]. The GA method repeatedly updates a population of individual solutions, by randomly selecting at each step, individuals within the updated population to be parents. These are utilized to produce the next generation children. In this way, the population evolves to an optimal solution [28].

The new approach proposed in this work is to combine a numerical computation of the electric field distribution around the insulator using a finite element solution and the application of the genetic algorithms method to realise the optimization of the insulator design and distribution of the electric field. After that, the obtained model is studied under polluted conditions by examining the electrical parameters (voltage, electric field and conduction current density distributions).

# 2 APPROACH AND MODEL PARAMETERS

## 2.1 PROPOSED APPROACH AND OPTIMISATION OF ELECTRIC FIELD DISTRIBUTION

The electric field distribution is one of the main factors which control current density and can initiate discharge development on the insulator surface. The electric field profile has peak regions, particularly near the metallic fittings at which dry bands are formed [29]. The optimized performance of a high voltage insulator is closely linked to the effective minimization of the electric field stress along its creepage length, especially around metallic fittings [30]. That is why a particular attention is given to the pin region at which the electric field magnitude is expected to be the highest. The highest electric field magnitude at the pin is used here as the objective function to be optimized (minimized) in the GA approach. So, for each step, the electric field magnitude value at the pin is calculated and then the GA method is used to compare it to the previous value until a minimum is achieved, which is the solution sought in this investigation. The GA is operated with satisfying two constraints simultaneously; keeping the creepage distance as well as the diameter of the insulator constant, thereby, only a change in insulator shape is introduced. This optimized model is studied in presence of wetted pollution represented as a thin conductive layer on the upper side of the insulator shed and as droplets of humid pollution in the lower part of the insulator ribs.

The electrical parameters including voltage, electric field and conduction current density distributions of this optimized model were investigated and, for each case, they were compared with the industrial cap and pin insulator shape used in practice.

## 2.2 MODEL PARAMETERS

Because of their reliability and their excellent resistance to material degradation, ceramic insulators are extensively used worldwide [2]. Compared with porcelain insulators, glass insulators with the same profiles were found to have better performances under pollution conditions [31].

The studied sample (Figure 1) is a glass cap and pin insulator F12AS type. Its electrodes are made of a cast iron cap, which is set to ground potential, and an energized steel pin. The insulating skirt is made of glass. The insulator has 4 under-shed ribs, numbered 1 to 4 in Figure 1 where $S_1$ refers to the upper surface of the insulating glass shed and $S_2$ refers to the surface of all the creepage length.
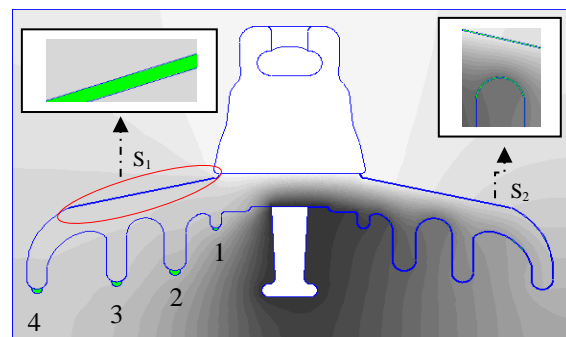


**Figure 1.** F12AS Type glass insulator depicting details of shape, pollution layer and water droplet formation on the ribs.

In order to reconstruct the shape of the insulator for use in the numerical computations, its profile is segmented into short sections identified by their lengths, curvatures, angles and arc lengths. Figure 2 shows details of the insulator sections and Table 1 gives a summary of the dimensions. The shed slope is $\beta=0.23$. The insulator geometric data are; the Diameter (d) =286 mm, Creepage distance (L) =421 mm, Spacing (p) = 146 mm, and its approximate weight=6.4 kg.
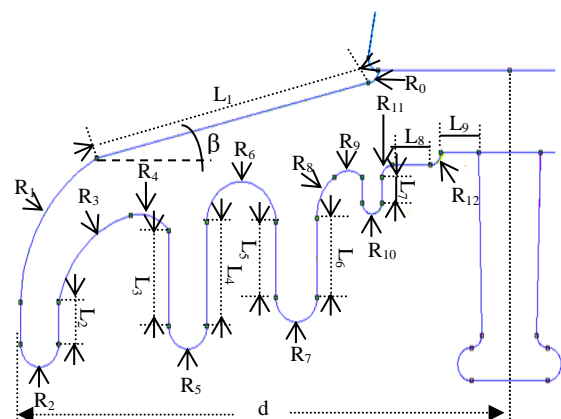


**Figure 2.** Details of the simulation model.

**Table 1.** Geometric parameters used for the model (see Fig. 2 for details).

| Radius (mm) | Angles (°) | Lengths (mm) |
|---|---|---|
| $R_0=3$ | $\varphi_0=90$ | $L_1=81$ |
| $R_1=42$ | $\varphi_1=60$ | $L_2=8.5$ |
| $R_2=5.5$ | $\varphi_2=180$ | $L_3=21.5$ |
| $R_3=21$ | $\varphi_3=63$ | $L_4=23.5$ |
| $R_4=11$ | $\varphi_4=61$ | $L_5=16$ |
| $R_5=5.5$ | $\varphi_5=180$ | $L_6=17$ |
| $R_6=10$ | $\varphi_6=180$ | $L_7=4.1425$ |
| $R_7=6$ | $\varphi_7=180$ | $L_8=10$ |
| $R_8=10$ | $\varphi_8=62$ | $L_9=11$ |
| $R_9=4$ | $\varphi_9=90$ | - |
| $R_{10}=3$ | $\varphi_{10}=180$ | - |
| $R_{11}=3$ | $\varphi_{11}=90$ | - |
| $R_{12}=3$ | $\varphi_{12}=90$ | - |

For the optimisation carried out in this paper, the modified shape needs to satisfy the objective which aims to minimize the highest value of the electric field located at the pin [11] while fulfilling the constraint of keeping constant both the creepage distance and the diameter of the insulator.

The electric field distribution is computed using FEMM [32] software which uses the finite element method. The electric currents module of FEMM in the frequency domain is used in combination with Matlab environment to solve the governing equations for:

$$\text{Electric field:} \vec{E} = -\vec{\nabla}V \tag{1}$$

And current density: $\vec{J} = \sigma\vec{E} + \varepsilon\,\partial\vec{E}/\,\partial\vec{t}$ (2)

where V: Electric potential, *E:* Electric field vector, J: Current density, $\sigma$ :Volume conductivity and $\varepsilon$:Dielectric constant.

The relative permittivity values used in the model are 5.59 for glass, 1 for air, and 80 for the water droplets and the pollution layer [33].

The following assumptions were made for the computation of electric field distribution:

a) The insulator shape is circular and symmetrical; the model is examined on a bi-dimensional space using axi-symmetry.
b) The study is focused on the outer insulating skirt, and all phenomena due to material properties are neglected.
c) Any discharge event that may appear due to high electric field magnitudes is ignored.
d) The effect of water droplet deformation due to the electric field stresses is neglected.

A number of pollution scenarios were considered to investigate their effect on the studied parameters, i.e. voltage, electric field and current density distributions: The scenarios consisted of depositing water droplets at the lower edges of the ribs as indicated in Figure 1. An electrical conductivity of 4.8 S/m (corresponding to sea salt) [34], was used for the water droplets, corresponding to a salinity between 28 and 40 kg/m³ at a temperature of 20°C [35]. The volume of the water droplets is taken as 48µl [33] for the droplets in positions 2,3 and 4 and 12 µl for the droplet in position 1. On the upper surface of the insulator $S_1$, a thin conductive pollution having 0.5 mm thickness is used to simulate humid contamination.
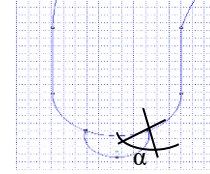
After this, the same pollution layer is deposited on the total surface $S_2$, of the insulator to simulate the case of a continuous pollution which is expected to be the most critical case.

Table 2 summarizes the eight scenarios investigated in this work, giving the locations where the droplets were deposited or when a thin pollution layer was used.

**Table 2.** The different scenarios of water droplet location and pollution configuration.

| Scenarios | 1 | 2 | 3 | 4 | 5 | 6 | 7 | 8 |
|---|---|---|---|---|---|---|---|---|
| Ribs | 1 | 2 | 3 | 4 | 12 | 1234 | -- | -- |
| Surfaces | - | - | - | - | - | - | S1 | S2 |

The simulation of water droplets on the surface of under-shed ribs of the insulator uses hemispherical droplet shapes with selected contact angles, α, between 55° and 66°. The range of contact angle is used to account for the hydrophilic property of ceramic insulators [15, 36-37]. Figure 3 shows a schematic of the droplet representation with contact angle definition.



**Figure 3.** Representation of water droplets and their contact angle with the insulator surface.

## 3   ELECTRIC FIELD RESULTS

For the GA method, the different lengths $L_2$, $L_3$, $L_4$, $L_5$, $L_6$ and $L_7$ (as shown in Figure 2) are taken as optimization variables that must satisfy equalities and inequalities constraints in Table 3.

**Table 3.** GA constraints

| Inequalities Constraint | Equalities Constraint |
|---|---|
| $1\text{ mm} \leq L_2 \leq 10\text{ mm}$ | $2*(L_2 + L_3 + L_5 + L_7) = 100.3\text{ mm}$ |
| $1\text{ mm} \leq L_3 \leq 30\text{ mm}$ | $L_4 = L_3 + 2\text{ mm}$ |
| $1\text{ mm} \leq L_5 \leq 26\text{ mm}$ | $L_6 = L_5 + 1\text{ mm}$ |
| $1\text{mm} \leq L_7 \leq 26\text{ mm}$ | |

In the GA model, minimization of the electric field at the insulator pin is used as the fitness function (Objective function). Therefore, for each calculation step, the electric field is computed at the pin, and the Genetic Algorithm compares it to the last value until it reaches a minimum, which is the solution sought, as shown in Figure 4.

As can be seen in Figure 5, a finer mesh is generated around the insulating skirt region to enhance the accuracy of computed values whilst for the air region, far from the insulating skirt, the mesh used is more coarse to reduce computation time. The metal electrodes were not meshed. For the numerical computation of electric field values, a per unit potential of 1 kV, 50 Hz was assigned to the pin.

A number of configurations were studied, and results were obtained depending on the number of chosen initial population and number of iterations performed, since the genetic algorithm uses random number generators. Two cases are shown in Table 4, where the changes were applied to the different ribs of the

insulators. As can be seen from the table, a further benefit of this optimization is realized through the reduction of the lateral surface of the insulator, hence, weight reduction of the insulator.
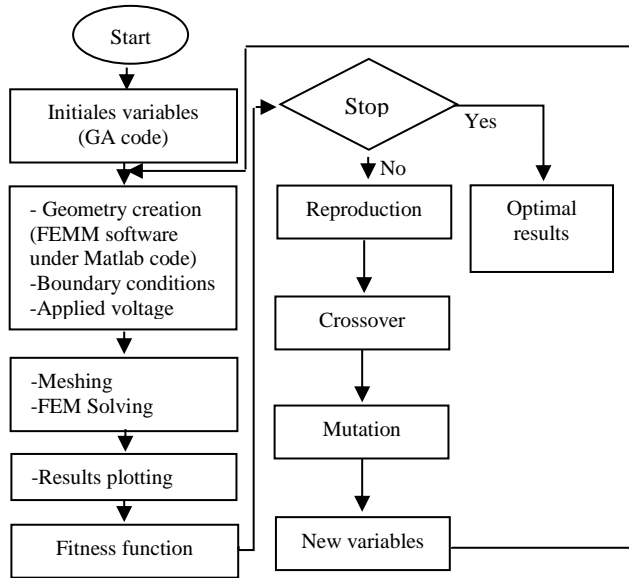


**Figure 4.** Schematic diagram of the Finite Element method combined with the Genetic Algorithm (GA).
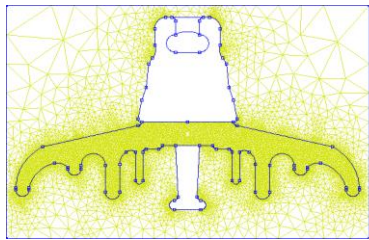


**Figure 5.** Meshed model used in Finite Element computations.

**Table 4.** Optimization results.

|  | F12AS Model | Optimized Model 1 | Optimized Model 2 |
|---|---|---|---|
| L2 (mm) | 8.5 | 1.9 | 5.6 |
| L3 (mm) | 21.5 | 1.1 | 17.1 |
| L4 (mm) | 23.5 | 3.1 | 19.1 |
| L5 (mm) | 16 | 23.1 | 7.6 |
| L6 (mm) | 17 | 24.1 | 8.6 |
| L7 (mm) | 4.1425 | 24.1 | 20 |
| Creepage distance (L) (mm) | 421 | 421 | 421 |
| Field value (kV/cm) | 1.84 | 1.55 | 1.55 |
| Surface (cm$^2$) | 73 | 71 | 72 |

From the models obtained in Table 4, Model 1 was chosen to perform a comparative study between the currently used F12AS insulator and the optimised insulator geometry determined through the GA method. The study was carried out for the different scenarios listed in Table 3.

## 3.1 CLEAN CASE

The computed equipotential distributions for the reference (industrial one) insulator and the optimized Model 1 are shown in Figures 6a and 6b respectively.
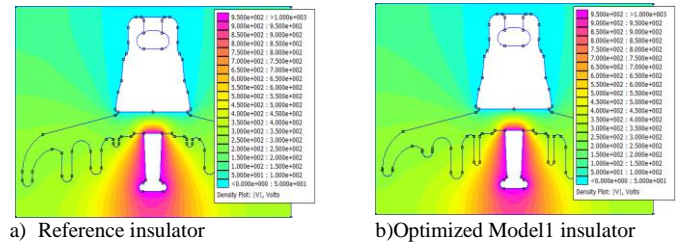


a)  Reference insulator          b)Optimized Model1 insulator

**Figure 6.** Equipotential distribution under clean surface conditions.

For the potentials and tangential electric field plots, a maximum 99999 points were selected to ensure better accuracy of the extracted curves. The electric potential distribution along the creepage distance of the two insulators for the clean insulator surface is given in Figure 7, with potential values varying between 0 kV at the cap to 1 kV at the pin.
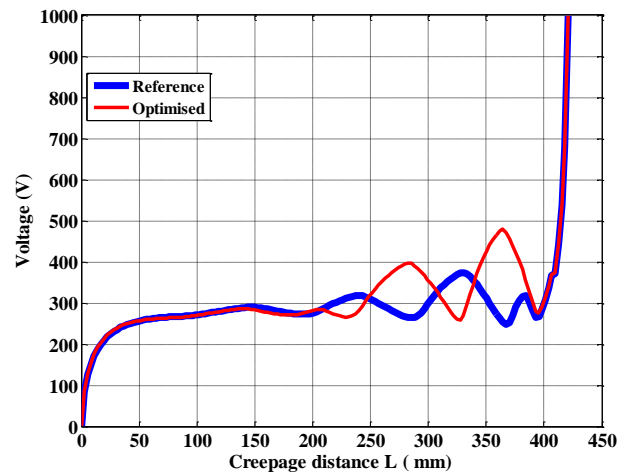


**Figure 7.** Potential distribution along the clean insulator profile for the standard and optimised Model 1 insulator shapes. (creepage path cap to pin)

Figure 8 shows the electric field distribution. As can be seen on Figures 7 and 8, both voltage and electric field are redistributed favourably using the GA optimised Model 1 shape. In Figure 8, the maximum electric field value on the pin was reduced from 1.84 kV/cm for the standard reference model to 1.55 kV/cm for the optimized Model 1 shape, equivalent to a 16% reduction. As expected, the voltage distribution on the insulator surface is highly non-linear, which leads to extremely high electrical stresses around the pin region. These stresses, in turn, may lead to dry band formation and initiation of surface discharges [38]. Close examination of the results in Figure 9, giving the tangential electric field distribution, reveal that the maximum tangential electric field magnitude is reduced for the case of the optimised Model 1 by as much as 13% compared to the standard insulator shape, with a lower value of 1.4 kV/cm compared with 1.6 kV/cm respectively.

Under clean surface conditions, there is no current flow on the surface, which prevents formation of dry bands and resulting surface discharges.
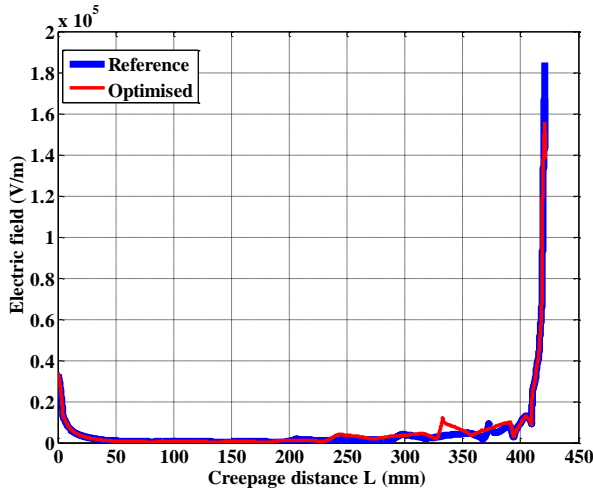


**Figure 8.** Electric field distribution along the clean insulator profile for standard and optimised Model 1 insulator shapes. (creepage path cap to pin)
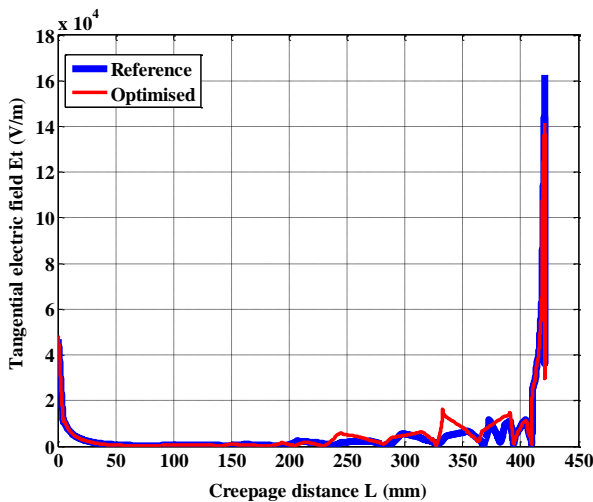


**Figure 9.** Tangential Electric field distribution along the clean insulator profile for standard and optimised Model 1 insulator shapes.

### 3.2 INSULATOR SURFACE WITH POLUTION

Surface discharges on outdoor insulators, due to wet pollution and dry band formation causes flow of leakage current on the insulator surface. Such mechanisms govern the design and performance of outdoor insulators. In this investigation, the different scenarios of pollution given in Table 3 were quantified.

The tangential electric field, which drives the leakage current along the insulator surface profile, was computed for all scenarios. Figures 10 to 15 report the distribution of the tangential electric field along the creepage distance for Scenarios 1 to 8, as described in Table 3.

• **In Scenario 1**, where just one droplet is deposited at Location 1 for the two insulators, a small increase in the tangential electric field distribution is observed for both

conventional and optimised models after introducing the polluted water droplet compared with the clean case (Figure 10a). The computed increases are 3% for the industrial insulator and 5% for the proposed optimized insulator shape. For the polluted case, the tangential electric field for the optimized model is decreased by 19% compared with the industrial model, indicating that the optimized model is more performant under pollution deposited near to the high voltage terminal. Figures 10b and 10c present the above results on a logarithmic scale to highlight the influence of the conductive water droplet on the tangential electric field around the water droplet region and near the high voltage terminal.

• **Scenario 2**: The water droplet is now moved to Location 2. In this case, the optimized model yields the same value, as for Scenario 1, for the electric field around the pin (Figure 11) with 1.3 kV/cm whilst an increase to 1.6 kV/cm for the industrial insulator is computed. For this Scenario, a field magnitude reduction is observed compared to the clean case for both models with a decrease of 3 % for the industrial insulator and 5% for the optimized shape.

• **Scenario 3**: For the third Scenario, the water droplet is moved to Location 3. In this case, any change in the maximum tangential electric field value is noticed compared with the case above.

• **Scenario 4**: In this case, the maximum electric field value around the pin remains the same as Scenarios2 and 3 above.

• **Scenario 5**: Two polluted water droplets are deposited at Locations 1 and 2 simultaneously. It can be observed that the optimized model performance is better than the industrial model, exhibiting a decrease of 19 % in the maximum tangential electric field with a value of 1.4kV/cm for the optimized model against 1.7 kV/cm for the industrial insulator (Figure 12).
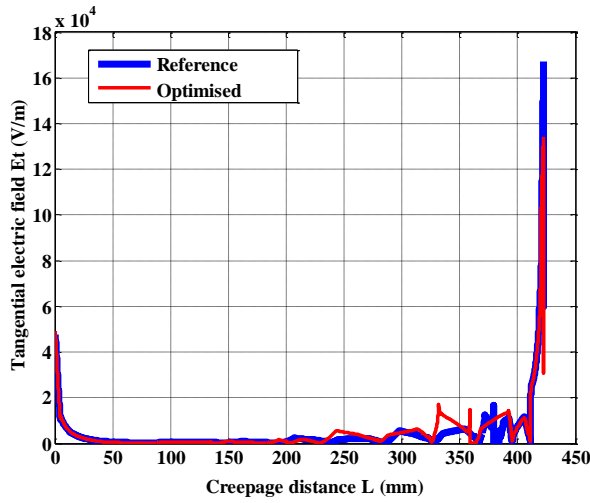
Compared with the clean case, the maximum tangential electric field value increases by 6 % for the industrial model but it decreases by 1.4% for the optimized shape.

• **Scenario 6**: At Locations 1, 2, 3 and 4, the maximum tangential electric field is practically the same for both models, with a decrease of 0.6% for the optimized model (Figure 13). Compared with the clean case, an increase in the maximum tangential electric field value is predicted for both models, with 6% for the industrial model and 21 % for the optimized insulator shape.
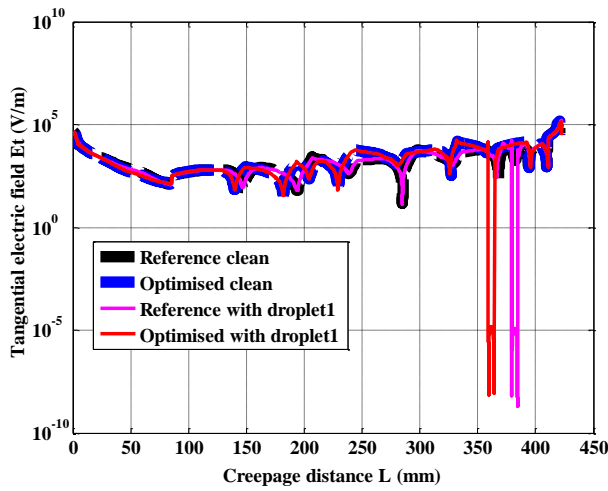
• **Scenario 7**: In this case, where a thin layer of humid pollution is deposited on the upper surface of the insulator shed $S_1$, we can observe a rise of 12% in the maximum tangential electric field for the optimized model compared with the industrial shape (Figure 14).

Compared with the clean case, no change is observable in the maximum tangential electric field for the industrial model but a significant rise of 29 % is computed for the optimized shape.
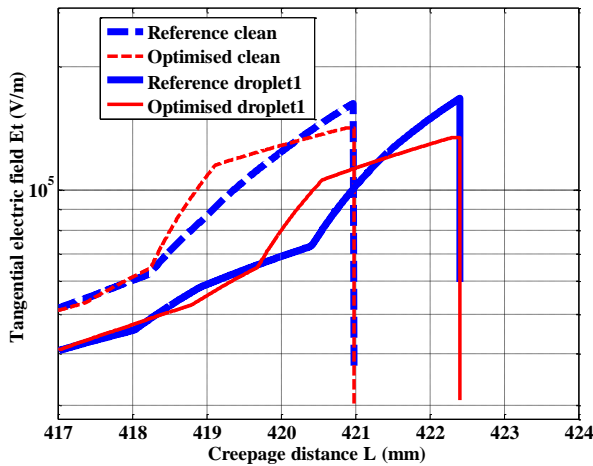
• **Scenario 8**: In the case of a continuous pollution layer $S_2$, it is observed that both models exhibit the same performance (Figure 15), and there is a significant decrease of the tangential electric field values compared with the clean case, with a maximum of 0.7 kV/cm near the ground fitting.

*a)* *Field along the creepage distance - linear scale*



*b)* *Field long the creepage distance - logarithmic scale*



*c)* *Field around the pin region- logarithmic scale*

**Figure 10.** Tangential electric field distribution along the creepage distance for Scenario 1 (droplet at location 1) for both model insulators.
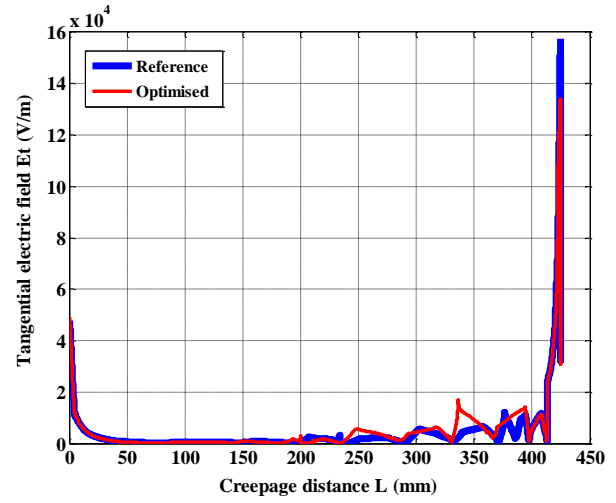


**Figure 11.** Tangential electric field along the creepage distance for Scenario 2 (droplet at location 2).
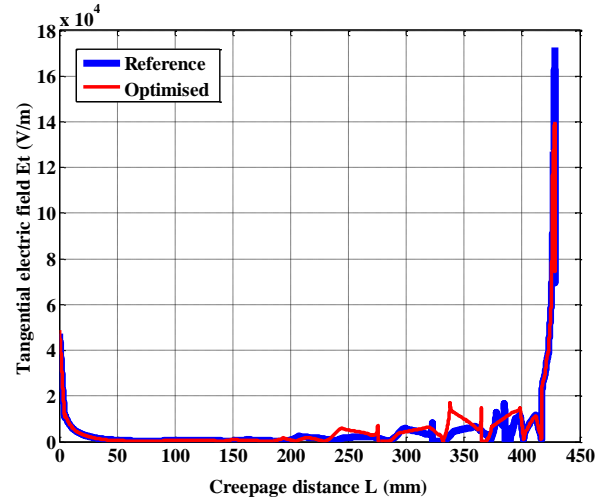


**Figure 12.** Tangential electric field along the creepage distance for Scenario 5 (polluted droplets 1 and 2).
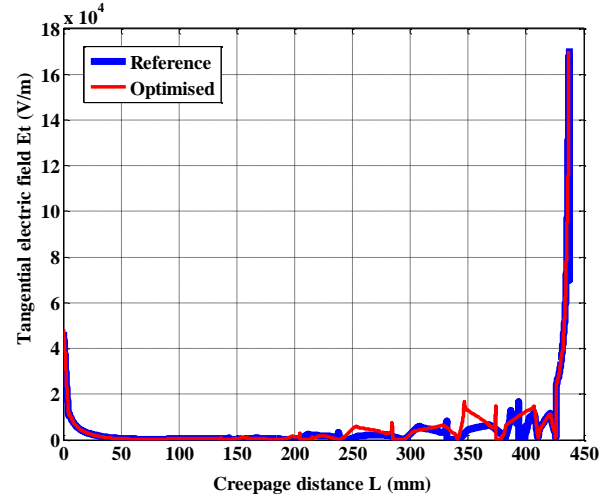


**Figure 13.** Tangential electric field along the creepage distance for Scenario 6 (droplet 1, 2, 3 and 4).
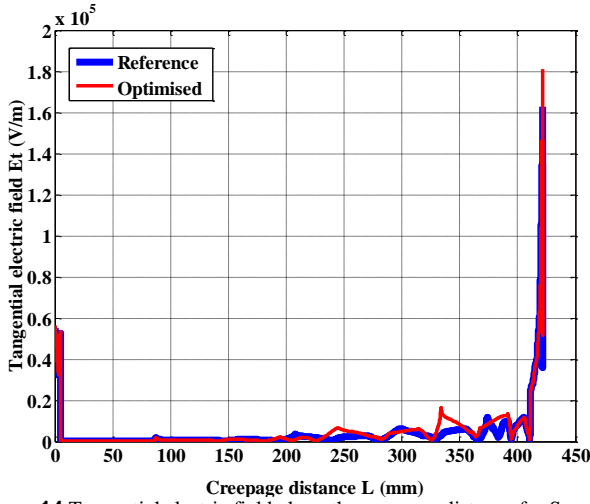
**Figure 14.**Tangential electric field along the creepage distance for Scenario 7 (pollution on upper surface of the insulator).
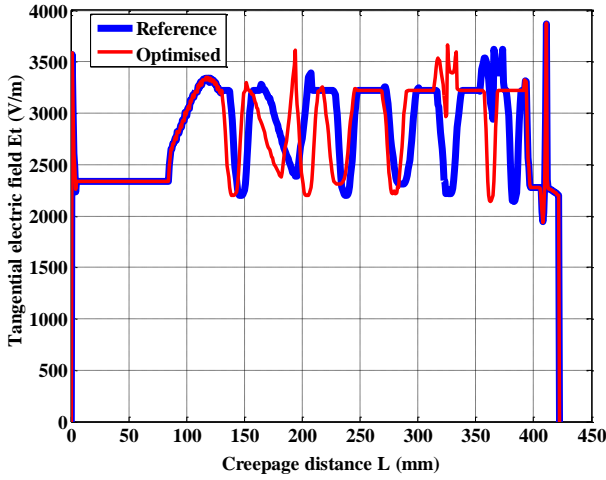


**Figure 15.** Tangential electric field along the creepage distance for Scenario 8 (continuous pollution layer on the surface of the insulator).

# 4 CONDUCTION CURRENT DENSITY

Failures in high voltage insulators is frequently initiated with the leakage current flow [39], and this important factor is considered in this investigation.

Figure 16 shows the leakage conduction current density distribution along the insulator profile for Scenarios 1 to 4. As can be seen, the leakage current density is only significant at the position of water droplets. Furthermore, it is observed that, when the droplets are closer to the end fittings, cap and pin, the magnitude of the leakage current density is higher. In Scenario 1, we observe a decrease in the leakage current density for the optimized model compared to the standard shape. This decrease is lower as the droplet is moved away from the pin, to become negligible for the case of Scenario 4.

Figure 17 shows the leakage current density distribution along the insulator profile for Scenario 6 (for droplets 1 to 4 at the same time), and it can be observed that it is identical to that seen on Figure 16. We can infer that the leakage current density at any water droplet is not influenced by the presence of other droplets in its surroundings.



**Figure 16.**Leakage current density distribution along the creepage distance with Scenarios 1, 2, 3 and 4.



**Figure 17.** Conduction current density distribution along the creepage distance with Scenario 6 (droplets at 1, 2, 3 and 4 locations simultaneously).

In the case of a continuous pollution layer on the upper shed $S_1$ (Scenario 7), Figure 18 indicates that the leakage current density is much higher and its distribution is almost similar for both models. Similar results were obtained for Scenario 8, as shown in Figure 19.



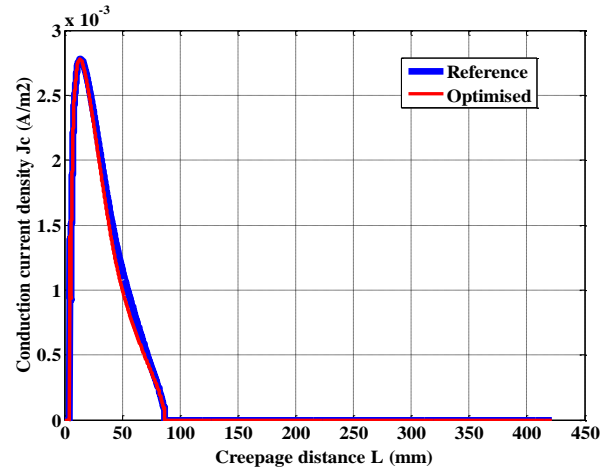**Figure18.** Conduction current density distribution along the creepage distance for Scenario 7 (pollution on upper surface $S_1$).
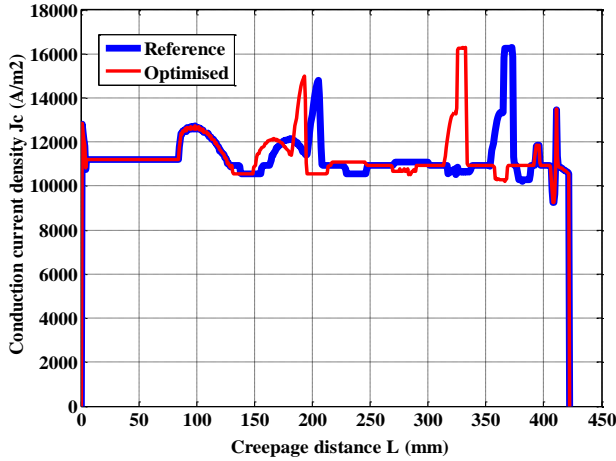
**Figure 19.** Conduction current density distribution along the creepage distance for Scenario 8 (pollution on upper surface $S_2$).

## 5  COMPARATIVE PERFORMANCE AND DISCUSSION

Table 4 summarises the computed results of tangential electric field magnitudes for the different scenarios to identify the advantages of the studied optimised insulator shape.

A comparison between the optimized model and the industrial insulator shape is given in the fourth column of Table 4, and a comparison between the clean polluted cases is shown in column 6.

It should be highlighted that, when the water droplets are near to pin (high voltage) as seen in Scenarios 1, 2, 3 and 4, the optimized shape is shown to give a better performance in terms of maximum tangential electric field. This points out that the optimized model can offer advantages under pollution conditions. However, when the pollution is located far away from the pin, as seen in Scenario 7, the industrial model exhibits superior performance.

**Table 4.** Comparison between the optimized and the industrial models using maximum electric field value.

| Scenarios | Models O(Optimized) I(Industrial) | Maximum electric field value kV/cm | Difference between I and O % | | Difference with the clean case % |
|---|---|---|---|---|---|
| 1 | I | 1.67 | -19.77 | + | +3.08 |
|   | O | 1.34 |  |  | +4.96 |
| 2 | I | 1.57 | -14.65 | + | -3.08 |
|   | O | 1.34 |  |  | -4.96 |
| 3 | I | 1.57 | -14.65 | + | -3.08 |
|   | O | 1.34 |  |  | -4.96 |
| 4 | I | 1.57 | -14.65 | + | -3.08 |
|   | O | 1.34 |  |  | -4.96 |
| 5 | I | 1.72 | -19.18 | + | -1.41 |
|   | O | 1.39 |  |  | +6.17 |
| 6 | I | 1.71 | -0.58 | + | +5.55 |
|   | O | 1.70 |  |  | 20.56 |
| 7 | I | 1.62 | +12.34 | - | 0% |
|   | O | 1.82 |  |  | +29.07 |
| 8 | I | 0.68 | 0% | = | +58.02 |
|   | O | 0.68 |  |  | +51.77 |

\* + indicates that the optimized model is better than the industrial shape

No significant improvement is observable for the case of a continuous pollution layer, as in Scenario 8.

Finally, it is noted that the shape of the optimized model approaches the profile of the anti-fog insulator design.

## 6  CONCLUSION

Applying the genetic algorithms method to the industrial cap-and-pin insulator shape using the mono-objective optimization, several shapes of the insulator can be obtained depending on the adopted number of initial population and iteration. All these shapes exhibit a reduced electric field value at the insulator pin where the electric field is maximum and where the risk of discharge initiation is highest. Furthermore, some of these shapes are characterised by reduced geometric dimensions compared with industrially adopted insulator shapes. Therefore, the weight may also be reduced.

To examine the performance of the so-obtained shapes after optimization under pollution conditions, wet pollution was deposited at different positions of the insulator ribs, and both the tangential electric field and current density were computed and compared for the various models.

An important result obtained in this study is related to the water droplets effect; when the water droplets are near to the high voltage fitting (pin), where the electric field is always highest, the so-determined optimised model performs better compared to existing insulators by lowering the electric field magnitude by up to 20%.

Similarity in shape of the optimised model with the anti-fog insulator profile is highlighted around the under shed ribs surrounding the pin.

### REFERENCES

[1] M. Farzaneh and W. A. Chisholm, "*Insulators for icing and polluted environments*". Piscataway, IEEE Press, John Wiley & Sons, Inc. Publication, 2009.

[2] A. P. Mishra, R. S. Gorur, and S. Venkataraman, "Evaluation of Porcelain and Toughened Glass Suspension Insulators Removed from Service", *IEEE Trans. Dielectr. Electr. Insul.*, Vol. 15, No. 2, pp. 467-475, Apr. 2008.

[3] M. T. Gençoğlu and M. Cebeci, "The pollution flashover on high voltage insulators", *Electr. Power Syst. Res.*, Vol. 78, No. 11, pp. 1914–1921, Nov. 2008.

[4] Waluyo, M. Parouli, Pakpahan, Suwarno, and M.A. Djauhari, "Study on Leakage Current Waveforms of Porcelain Insulator due to Various Artificial Pollutants", *Int. J. Electr. Comput. Energ. Electron. Commun. Eng.*, Vol. 1, No. 8, pp. 1135-1140, 2007.

[5] P. J. Lambeth, "Effect of pollution on high-voltage outdoor insulators", *Proc. IEE, IEE Rev.,* Vol. 118, No. 9, pp. 1107–1130, 1971.

[6] CIGRE Task Force 33.04.01, "Polluted Insulators: A review of current knowledge", CIGRE Technical brochure 158, Jun.2000.

[7] R. Boudissa, S. Djafri, A. Haddad, R. Belaicha, and R. Bearsch, "Effect of insulator shape on surface discharges and flashover under polluted conditions", *IEEE Trans. Dielectr. Electr. Insul.*, Vol. 12, No. 3, pp. 429–437, 2005.

[8] N. Bashir and H. Ahmad, "Ageing of transmission line insulators: The past, present and future", *IEEE Conf. Power and Energy*, pp. 30–34Johor Baharu, Malaysia, December .2008.

[9] S. C. Oliveira, E. Fontana, and F. Cavalcanti, "Real time monitoring of the leakage current of 230 kV insulator strings under washing", *IEEE/PES Transmission and Distribution Conference and Exposition*, , pp. 1–4, 2008.

[10] A. Haddad and D. Warne, "*Advances in High Voltage Engineering"*, London, UK, IET, CH.6, pp.296-300, 2004.

[11] S.M. Braini, "Coatings for outdoor high voltage insulators", PhD Thesis, School of Engineering, Cardiff University, 2013.

[12] E. A. Cherney and R. S. Gorur, "RTV Silicone Rubber Coatings for Outdoor Insulators", *IEEE Trans. Dielectr. Electr. Insul.*, Vol. 6, No. 5, pp. 605–611, Oct. 1999.

[13] P. Claverie and Y. Porcheron, "How to choose insulators for polluted areas", *IEEE Trans. Power Appar. Syst.*, No. 3, pp. 1121–1131, 1973.

[14] M.T.Gerardo, H.C.Ramiro, and R.V.Isa´ıas, "Experiences on pollution level measurement in Mexico", *Electr. Power Syst. Res.*, vol. 76, no. 1–3, pp. 58–66, Sep. 2005.

[15] Suwarno,A. Basuki, F. Lendy and Sumedi, "Improving outdoor insulator performances installed at coastal area using silicone rubber coating",*Int'l.Conf. on Condition Monitoring and Diagnosis (CMD),*pp. 1143–1146, Bali, Indonesia,2012.

[16] N. Dhahbi-Megriche, A. Beroual, and L. Krähenbühl, "A new proposal model for flashover of polluted insulators", *J. Phys. Appl. Phys.*, Vol. 30, No. 5, pp. 889-894, 1997.

[17] A. Haddad, P. T. Waters, H. Griffiths, K. Chrzan, N. Harid, P. Sarkar and P. Charalampidis, "A new approach to anti-fog design for polymeric insulators", *IEEE Trans. Dielectr. Electr. Insul.*, Vol. 17, No. 2, pp. 343–350, 2010.

[18] N. Hayakawa, J. Shimomura, T. Nakano, M. Hanai, K. Kato, and H. Okubo, "Fabrication technique of permittivity graded materials (FGM) for disk-type solid insulator", *Annual Report Conf.* Electr. Insul. Dielectr. Phenomena, *(CEIDP),* pp. 32–35, 2012.

[19] W. S. Chen, H. T. Yang, and H. Y. Huang, "Contour Optimization of Suspension Insulators Using Dynamically Adjustable Genetic Algorithms", *IEEE Trans. Power Deliv.,* Vol. 25, No. 3, pp. 1220–1228, 2010.

[20] B. M'hamdi, M. Teguar, and A. Mekhaldi, "Optimal design of corona ring on HV composite insulator using PSO approach with dynamic population size", *IEEE Trans. Dielectr. Electr. Insul..* Vol. 23, No. 2, pp. 1048–1057, 2016.

[21] D.Nie, H. Zhang, Z. Chen, X. Shen, and Z. Du, "Optimization design of grading ring and electrical field analysis of 800 kV UHVDC Wall bushing", *IEEE Trans. Dielectr. Electr. Insu.l*, Vol. 20, No. 4, pp. 1361–1368, 2013.

[22] W. S. Chen, H.T. Yang, and H. Y. Huang, "Optimal Design of Support Insulators Using Hashing Integrated Genetic Algorithm and Optimized Charge Simulation Method", *IEEE Trans. Dielectr. Electr. Insul.*, Vol. 15, No. 2, pp. 426–434, 2008.

[23] K. Bhattacharya, S.Chakravorti, and P. K. Mukherjee, "Insulator Contour Optimization by a Neural Network", *IEEE Trans. Dielectr. Electr. Insul.*, Vol. 8, pp. 157–161, 2001.

[24] S. Banerjee, A. Lahiri and K. Bhattacharya, "Optimization of Support Insulators Used in HV Systems Using Support Vector Machine", *IEEE Trans Dielectr. Electr. Insul.*, Vol. 14, pp. 360–367, 2007.

[25] IEC/TS 60815-1, "Selection and dimensioning of high-voltage insulators intended for use in polluted conditions", 2008.

[26] S. N. Sivanandam and S. N. Deepa, "*Introduction to genetic algorithms"*, Berlin ; New York: Springer, 2007.

[27] I. F. Gonos, F. V. Topalis, and I. A. Stathopolos, "Genetic algorithm approach to the modelling of polluted insulators", *IEE Proc. - Gener. Transm. Distrib.*, vol. 149, no. 3, p. 373, 2002.

[28] The MathWorks, *Genetic Algorithm and Direct Search Toolbox User's Guide*. 2004.

[29] R. Abd Rahman, "Investigations of ZNO microvaristor for stress control on polymeric outdoor insulators", PhD Thesis, School of Engineering, Cardiff University, Aug-2012.

[30] V. Peesapati, C. Zachariades, Q. Li, S. M. Rowland, I. Cotton, F. Allison, D. Chambers, P. Rhodes, "Electric field computation for a 400 kV composite cross-arm", IEEE Conf. Electr. Insul. Dielectr. Phenomena*, Annual Report Conference*, pp. 790–793, 2012.

[31] X. Jiang, J. Yuan, L. Shu, Z. Zhang, J. Hu, and F. Mao, "Comparison of DC Pollution Flashover Performances of Various Types of Porcelain, Glass, and Composite Insulators", *IEEE Trans. Power Deliv.*, Vol. 23, No. 2, pp. 1183–1190, 2008.

[32] D. Meeker, *Finite element method magnetic, User's manuel*. 2006.

[33] A. J. Phillips, D. J. Childs, and H. M. Schneider, "Aging of nonceramic insulators due to corona from water drops", *IEEE Trans. Power Deliv.*, Vol. 14, No. 3, pp. 1081–1089, 1999.

[34] A. C. Baker, M. Farzaneh, R. S. Gorur, S. M. Gubanski, R. J. Hill, G. G. Karady, and H. M. Schneider, "Insulator Selection for AC Overhead Lines With Respect to Contamination", *IEEE Trans. Power Deliv.*, Vol. 24, No. 3, pp. 1633–1641, 2009.

[35] BS EN 60507, "Artificial pollution tests on high-voltage ceramic and glass insulators to be used on a.c. systems", 2014.

[36] S. Kumagai and N. Yoshimura, "Leakage current characterization for estimating the conditions of ceramic and polymeric insulating surfaces", *IEEE Trans. Dielectr. Electr. Insul.*, Vol. 11, No. 4, pp. 681–690, 2004.

[37] Suwarno, F. Pratomosiwi, "Application of RTV Silicone Rubber coating for improving performances of ceramic outdoor insulator under polluted condition", *Int'l. Conf. on Electrical Engineering and Informatics*, Vol. 2, pp. 581–587, 2009.

[38] S. Ganga, M. Kanyakumari, and R. S. Aradhya, "FEM approach to design functionally graded transformer bushing", *IEEE 10ᵗʰ Int'l. Conf.onProperties and Applications of Dielectric Materials (ICPADM)*, pp.1–3, 2012.

[39] M. El-Shahat and H. Anis, "Risk assessment of desert pollution on composite high voltage insulators", *J. Adv. Res.*, Vol. 5, No. 5, pp. 569–576, 2014.

**D. Doufene** Graduated in 2008 from the University Of Science and technology Houari Boumédienne (USTHB), Algeria with a degree of "Ingeneieur d'Etat" and then obtained the "Magister" degree from USTHB, Algeria in 2010. She is now pursuing the Ph.D. degree in high voltage engineering in the LSEI laboratory of USTHB University.

Her research areas are mainly on high voltage technology, outdoor insulation, optimization problems and artificial intelligence.

**S. Bouazabia,** has obtained a first degree in electrical engineering in 1988, and a Ph.D. degree in high voltage engineering in 2006 from Ecole National Polytechnique (ENP) of Algiers. He is now a Professor in electrical engineering at Houari Boumédiene Univesity. His research interests are in insulation coordination and high voltage modeling.

**A. Haddad** obtained a first degree in Electrical Engineering in 1985 and then a Ph.D. degree in High Voltage Engineering in 1990. He is now a Professor at Cardiff University. His research interests are in overvoltage protection, insulation systems, insulation coordination and earthing systems. He has published an IET-Power Series Book on "Advances in High Voltage Engineering". He is a member of CIGRE working groups and a member of BSI PEL1/2, IEC TC37.

He serves on the scientific committees of several international conferences. He is a Fellow of the IET and a Fellow of the Learned Society of Wales.